WILEY InterScience® DISCOVER SOMETHING GREAT

PROTEINS STRUCTURE ■ FUNCTION ■ BIOINFORMATICS

RESEARCH COMMENTARY

Copper binding sites in the C-terminal domain of mouse prion protein: A hybrid (QM/MM) molecular dynamics study

Maria Carola Colombo,[1] Joost VandeVondele,[2] Sabine Van Doorslaer,[3] Alessandro Laio,[2] Leonardo Guidoni,[1] and Ursula Rothlisberger[1]*

[1] Laboratory of Computational Chemistry and Biochemistry, Institute of Chemical Sciences and Engineering, EPFL, CH-1015 Lausanne, Switzerland

[2] Laboratory of Inorganic Chemistry, ETH Hönggerberg-HCI, CH-8093 Zürich, Switzerland

[3] Department of Physics, University of Antwerp, Universiteitsplein 1, B-2610 Wilrijk, Belgium

ABSTRACT

We present a hybrid QM/MM Car–Parrinello molecular dynamics study of the copper-loaded C-terminal domain of the mouse prion protein. By means of a statistical analysis of copper coordination in known protein structures, we localized the protein regions with the highest propensity for copper ion binding. The identified candidate structures were subsequently refined via QM/MM simulations. Their EPR characteristics were computed to make contact with the experimental data and to probe the sensitivity to structural and chemical changes. Overall best agreement with the experimental EPR data (Van Doorslaer et al., J Phys Chem B 2001; 105: 1631–1639) and the information currently available in the literature is observed for a binding site involving H187. Moreover, a reinterpretation of the experimental proton hyperfine couplings was possible in the light of the present computational findings.

Proteins 2008; 70:1084–1098.

Key words: copper-binding protein; molecular simulations; Creutzfeldt–Jacob disease; EPR; ENDOR.

INTRODUCTION

The PrP is a widespread cell surface tethered protein expressed mainly in the tissues of the central nervous system. A conformational isomer of PrP^{c}, denoted as PrP^{Sc}, is believed to be responsible for a group of neurodegenerative diseases including Creutzfeldt–Jacob in humans, bovine spongiform encephalopathy (BSE) in cattle and scrapie in sheep.[1]

The NMR structures of prion proteins from different organisms[2,3] have become available, and more recently few X-ray structures[4,5] have also been determined. All structures are characterized by the presence of a globular, folded C-terminal domain (roughly 110 residues) and a flexible, *in vitro* unfolded N-terminal domain (roughly 90 residues). The latter is formed by a highly conserved repeat of four identical octapeptide units containing one histidine residue each.

In spite of continuing efforts aimed at the elucidation of the physiological function of the prion protein, its biological role has as yet remained elusive.

Abbreviations: ENDOR, electron nuclear double resonance; EPR, electron paramagnetic resonance; HA, helix A; HB, helix B; HC, helix C; HYSCORE, hyperfine sublevel correlation spectroscopy; MD, molecular dynamics; MM, classic mechanics; NMR, nuclear magnetic resonance; PDB, protein data base; PrP, prion protein; PrP^{c}, cellular prion protein; PrP^{Sc}, scrapie prion protein; QM, quantum mechanics; QM/MM, mixed quantum-classical calculations; RMSD, root mean square deviation.

Grant sponsor: Swiss National Science Foundation and the Italian National Research Council.
Joost VandeVondele's current address is University of Zurich, Physikalisch-Chemisches Institut, Winterthurerstrasse 190, 8057 Zurich, Switzerland.
Alessandro Laio's current address is International School for Advanced Studies (SISSA), Statistical and Biological Physics sector, via Beirut 2-4, I-34014, Trieste, Italy.
Leonardo Guidoni's current address is Dipartimento di Fisica, Ed. Fermi, Università degli Studi di Roma "La Sapienza", 00185 Roma, Italy.
*Correspondence to: Ursula Rothlisberger, Laboratory of Computational Chemistry and Biochemistry, Institute of Chemical Sciences and Engineering, BCH-4121, EPFL, CH-1015 Lausanne, Switzerland.
E-mail: ursula.roethlisberger@epfl.ch
Received 5 November 2006; Revised 15 February 2007; Accepted 28 March 2007
Published online 17 September 2007 in Wiley InterScience (www.interscience.wiley.com). DOI: 10.1002/prot.21604

Nevertheless, several contributions have pointed to a key role of PrP^c in copper metabolism[6] and a number of reviews are available on this topic.[7–10] In particular, the ability of PrP^c to bind Cu^{2+} *in vivo* and *in vitro*,[6,11–14] together with the promotion of PrP^c endocytosis for high copper concentrations,[15] suggest a role in copper homeostasis and transport.[15–17] In addition, a redox protective role,[12,18,19] or a superoxide dismutase (SOD)-like activity have also been proposed[19–22] and partially disproved.[23,24]

Up to recently, most of the biophysical investigations of copper binding to PrP^c have focused on the octarepeat region by means of different experimental techniques including electron paramagnetic resonance spectroscopy (EPR),[11,25–27] Raman spectroscopy,[28] circular dichroism,[29] mass spectroscopy (MS),[30] and X-ray spectroscopy.[31] The majority of investigations suggest that, in a pH range between 5 and 7, four copper ions are taken up in this domain.[11,13,26] A fifth copper ion has been proposed to bind to PrP in the region connecting the unstructured segment with the globular portion of the protein [PrP-(91–115)].[6,14,26,30,31]

Recent experiments have shown that Cu(II) also binds to the structured C-terminus [PrP-(123-231)][32–34] without substantial change in the protein conformation upon metal binding.[32] The Cu-binding sites in the full-length murine PrP, as well as in the C-terminal domain PrP(121–231) and in the N-terminal fragment PrP(58–91) alone have been probed by means of pulse EPR and electron nuclear double resonance (ENDOR) spectroscopy. Three pH-dependent Cu-binding modes were identified in the folded C-terminal domain. For the one dominant at physiological pH (complex **2**, pH 3–8) a histidine is coordinated to the copper ion and interactions with exchangeable as well as nonexchangeable protons are observed. The EPR parameters obtained for this complex are in good agreement with the ones reported for a complex of Cu(II) with a peptide fragment [PrP(180–193)][35] that spans HB (Fig. 1), suggesting the possible involvement of His187 in the coordination environment. However, information based on fragment studies should be evaluated with caution.[7] At lower pH (complex **1**, pH 3–6), the involvement of aspartic and glutamic acids is hypothesized, whereas the direct coordination to nitrogen atoms is ruled out by ENDOR and HYSCORE spectra.

On the other end, other experiments using a variety of techniques[16,26,30,36,37] could not identify any Cu-binding sites in the folded C-terminal domain. In spite of the controversies about the location of the copper ion, the findings that all of the disease-related mutations known lie within the residue interval 90–231, and that the mice expressing a truncated version of PrP with the octarepeat removed are still susceptible of prion infection although with longer incubation time,[38] confirm the pivotal role played by this part of the protein in PrP related diseases.

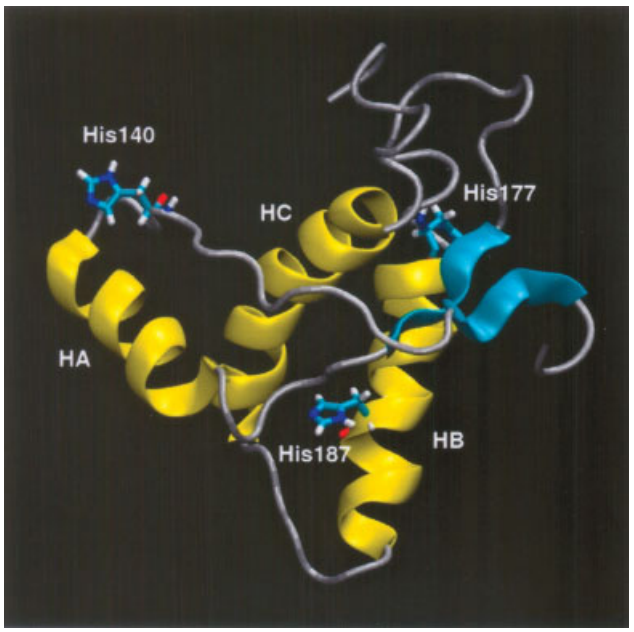

Figure 1
The C-terminal domain of the mouse PrP(124–226).[2]

Although a number of findings support the existence of a link between scrapie infection and copper metabolism, the actual molecular role of this metal ion is still under debate. Disturbances in the levels of Cu content have been suggested for prion-infected brain tissue[39,40] and a change in copper concentration was shown to influence incubation times for prion diseases.[41] Furthermore, a copper chelation therapy is able to slow down the infection progress in infected mice.[41] The elimination of the copper binding octarepeat region slows down disease progression[38] and copper-catalyzed redox damage is observed during prion disease.[42] The pro-aggregation effect of Mn(II) *in vitro* is blocked by a nanomolar concentrations of Cu(II) suggesting a significant effect of the metal on PrP conformation and stability.[43] These findings have lead to the hypothesis that the interplay of PrP with copper ions may have an important role in neurodegeneration processes.[7]

To shed some light on the controversial topic of copper binding sites and to provide specific data that can help probing putative sites, we performed a theoretical characterization of the structural and chemical properties of the copper loaded C-terminal domain of the mouse prion protein [PrP(124–226)].[2] Computational studies of PrP have so far been limited to classical MD simulations of the metal-free C-terminal domain[44–48] or portions of it.[44,49,50] The binding of open-shell transition-metal ions can imply strong polarization, and charge transfer effects and different coordination geometries that are not

easily described within standard force fields. In many cases, an adequate treatment can only be performed with an explicit quantum mechanical electronic-structure calculation. In addition, the problem of locating transition metal binding sites in proteins also necessitates the use of an approach that is able to take the entire protein environment into account and to incorporate finite temperature effects that are known to be crucial for biological function.[51] In order to fulfill all of the three conditions mentioned earlier, we apply a QM/MM Car–Parrinello simulation approach[52] that turned out to be successful in the treatment of a number of metal-containing systems.[53–55]

By means of a statistical analysis of the copper coordination in known protein structures, we localized the protein regions with the highest propensities for copper ion binding. Purely classical MD runs were performed as pre-equilibration for systems where coordination was only possible upon larger conformational changes (e.g., changes of backbone dihedral angles). Subsequently, the identified regions were refined via QM/MM Car–Parrinello simulations[52] in which the area around the copper ion was treated at the gradient corrected density functional level whereas the rest of the protein and the solvent were described via the classical force field GROMOS96.[56] For the putative coordination sites that emerged in this way, extensive calculations of the EPR parameters were undertaken using the Amsterdam Density Functional (ADF2002.01) package[57–59] to make contact with the experimental data in a semi-quantitative way and to probe the sensitivity to structural and chemical changes. The most likely binding site that does not violate the experimental findings involves H187. Furthermore the theoretical results suggest a reconsideration of the experimental data of the proton hyperfine couplings.[33]

METHOD

Statistical analysis and identification of candidate binding regions

We carried out a statistical analysis on a pool of known copper-binding proteins to identify the residues that most likely bind a copper ion. For this purpose, 207 PDB structures of copper proteins known at resolution $\leq$2.0 Å have been analyzed, yielding information about 383 copper binding sites and involving bonding to 1647 donor atoms (1563 amino acid atoms, 84 water oxygen atoms). The resulting coordination numbers indicate that some of the copper sites are under-coordinated in the PDB structures, probably because of the presence of labile water ligands that have not been resolved in the X-ray structures. The calculated relative probability for different amino acids that are involved in copper binding is shown in Table I, together with their average occurrence in proteins.[60] As could be expected, this statistical analysis shows that His is the most probable copper ligand and the coordination via Nε2 and Nε1 is essentially equally probable (53.4% and 46.3%, respectively). The second favorite copper ligand is Cys (binding via Sγ), followed by Met (binding via Sδ), Asp [binding via the carboxylic oxygen (82.6%), N (17.4%)] and Glu (binding via the carboxylic oxygen (80%), O (13.4%), N (6.7%). On the other end, the overall probability for coordination to an amide nitrogen (as suggested for the octarepeat sequence[17]) is only 0.4%. This probability pattern is largely different from the natural abundance of the amino acids. His, Cys, and Met residues together constitute about 92% of the copper ligands, whereas their natural abundance is less than 7%.

Table I
Relative Abundance of Copper Ligands in the PDB Structures Analyzed and Amino Acids Average Occurrence in Proteins[a]

aa	Relative abundance (%)	Average occurrence in proteins (%)
His	73.9	2.3
Cys	14.4	1.9
Met	3.8	2.2
Asp	1.2	5.3
Glu	0.8	6.3
Gly	0.2	7.2
Tyr	0.2	3.2
Ser	0.2	6.8

[a]For details concerning the pool of copper-proteins analyzed, see text. The amino acids average occurrence in proteins is reported from Ref. 60.

This probability map was used to scan through the NMR structure of the C-terminal domain of the mouse PrP(124–226) (PDB code 1AG2)[2]. In this search process the possible flip of the His imidazole plane was considered if it was enabling interactions with others likely coordinating residues. The regions with high probability for Cu-binding were identified and ranked according to the copper binding likelihood of the involved residues. Since all the highly ranked sites involve one of the three His residues of the C-terminal domain, we will refer to them as the H140, H177, and H187 binding sites. For every putative binding site, we have considered the possible participation of amino acid ligands in an extended region around the copper ion and if coordination was only possible upon larger conformational changes (e.g., changes of backbone dihedral angles), we have performed purely classical pre-equilibration runs on the time scale of 500 ps-1 ns after having positioned the copper ion. In particular, we used the GROMOS96 force field in combination with a P3M scheme to treat long range electrostatic interactions[61] with a grid of 64^3 points. The protein has been solvated using 4087 SPC water molecules at standard density. Initially the water molecules have been equilibrated with a fixed protein structure, performing purely classical MD for 150 ps at 300 K, with a box of 4.5 $\times$

DOI 10.1002/prot

5.9 × 5.2 nm^3. Afterwards, the entire system was equilibrated at 300 K for 150 ps.

For the H187 binding site, two classical MD runs were carried out with and without Cu-His(Nε2) restraints and resulted in two similar binding sites except for the side chain of E196 or D202 participating in the coordination spheres. Throughout the text, we will distinguish these two binding sites via the labels H187_E and H187_D, respectively.

QM/MM Car–Parrinello calculations

All the systems were partitioned into two regions, treated respectively at the QM and MM level. To saturate chemical bonds crossing the QM/MM interface we have parameterized a monovalent pseudo-potential for bond cuts[52] that has been successfully used in other systems.[53–55]

The copper ion, the side chain of the His characterizing the binding site, all the other potential ligands and, if necessary, water molecules are treated at the QM level. The composition of the QM region is adjusted during the dynamics if needed. If not differently specified the boundary pseudo-potentials are located on the Cβ of the involved residues.

The temporal evolution of the binding site involving His140 was studied starting from two different setups, involving the same ligands apart from the presence of Met138 (H140_M binding site) or Asp144 (H140_D binding site). The latter binding site was also probed after protonation of both the imidazole nitrogen atoms (H140_DD) as a putative model for the low pH form (complex **1**[33]).

The starting frame of the QM portion of the H140_M binding site includes the side chains of M138 and D147 whereas the H140_D binding site includes Asp144, Asp147 side chains and two water molecules (H_2Oa, H_2Ob). The QM portion of the H177 binding site involves the side chain of E178 and four water molecules (H_2Oc, H_2Od, H_2Oe, H_2Of). The QM portion of the H187_E binding site includes the side chains of E196, M206, and T191 (boundary atom pseudo-potential located on Cα), the backbone from Y157(Cα) to R156(Cα) and two water molecules (H_2Og, H_2Oh). The H187_D binding site includes the side chains of D202 and M206, the backbone from Y157(Cα) to R156(Cα) and two water molecules (H_2Oi, H_2Oe). To cut the Y157(N)—Y157(Cα) bond we have developed an optimized boundary atom pseudo-potential able to recover Y157(Cα) properties.

For the QM part of the QM/MM calculations we carried out DFT-based Car–Parrinello MD at a temperature of 300 K using the velocity rescaling algorithm for the initial temperature control. The time step used was 5 a.u. and the fictitious electronic mass μ = 500. The system is described with a spin polarized formalism, using the BLYP functional for the exchange and correlation.[62,63] The basis set for the valence electrons consists of plane waves expanded up to a cutoff of 80 Ry. The interactions between valence electrons and ionic cores are described by norm-conserving pseudo-potentials of the Martins–Trouiller type.[64] The QM supercell has dimensions of 13.8 × 13.8 × 13.8 $Å^3$ for the H140 binding site, 14.0 × 14.0 × 12.2 $Å^3$ for the H177 binding site, 14.0 × 15.5 × 15.6 $Å^3$ for the H187_E binding site and 16.1 × 15.1 × 14.3 $Å^3$ for the H187_D binding site. The charged QM regions were treated as isolated systems using the method by Martyna and Tuckerman.[65] The electrostatic interactions between quantum and classical regions are described within a fully Hamiltonian coupling scheme according to the method reported in Refs. 52 and 66.

Computation of EPR parameters

Since the time scale of EPR experiments is orders of magnitude larger than that of molecular vibrations, the result of the experiment is a Boltzmann average over all nuclear positions accessible to the dynamics during the experimental time window. Therefore, to approximate such an average we collected a number of snapshots along the dynamics to compute the EPR parameters. More specifically, 10 snapshots have been extracted from each trajectory after binding site equilibration at time intervals of 0.35 ps.

The EPR parameters were calculated on cluster models with the ADF2002.01 software package[57–59] using the method developed and implemented by Van Lenthe *et al.*[67,68] Following the procedure suggested by Saladino and Larsen,[69] to compute the **g** matrix and the anisotropic component of the **A** matrix ($\mathbf{A_D}$ matrix) we performed scalar-relativistic spin-restricted open shell Kohn–Sham calculations with spin-orbit coupling (SO+SR ROKS). For the isotropic component of the **A** matrix (a_{iso}) we used scalar-relativistic spin-unrestricted open shell Kohn–Sham calculations (SR UKS).

The choice of the density functional and the basis set used in the EPR parameter computations have been extensively tested on model systems (data not shown). In particular, the chosen criterion was the agreement with the experimental hyperfine coupling constants for the prototype complex $[Cu(NH_3)_n]^{2+}$ (n = 4, 5, 6) in water as well as numerical convergence with respect to the basis set size. As for the size of the system to be included in the EPR calculations, it is important to stress that the spin density is a rather localized property and therefore it is expected to be well described in the framework of cluster calculations. Indeed, the environmental effect was previously found not to influence the computed EPR parameters significantly.[70,71] The inclusion of the second coordination shell did not change the EPR parameters for the prototype complex $[Cu(NH_3)_n]^{2+}$ as well as for some of the PrP copper binding sites. Accordingly, the

cluster models include the first copper coordination shell only. For the exchange-correlation functional, we used the VWN[72] local density approximation augmented with the generalized gradient corrected approximation for exchange by Becke[62] and by Perdew for correlation.[73] All electron calculations with QZ4P basis sets (core triple-ζ basis of Slater-type orbitals, valence quadruple-ζ with 4 sets of polarization functions) have been carried out. Relativistic effects have been included using the zero order relativistic approximation (ZORA)[74–76] and relativistic atomic potentials have been generated with the program DIRAC, supplied with the ADF2002.01[57–59] program package.

HYSCORE spectra

The experimental procedure followed to obtain the HYSCORE spectra reported in Figure 6 is described in Ref. 33.

RESULTS

Mixed QM/MM calculations

H140_M binding site

This binding site is located on a solvent exposed side of the protein in the proximity of the loop formed by the coil preceding HA and HA itself (Fig. 1). The role of this helix in the process of misfolding is still controversial; possible roles as a nucleus of the conversion or as a barrier for the same process have been suggested (Ref. 49 and references therein). The putative binding site identified in proximity of H140 involves M138 and D147. During the MM relaxation both of the D147 carboxylic oxygen atoms enter the copper coordination sphere whereas the Met is located in an unfavorable orientation for coordination with respect to the lone pair of the sulphur atom. The QM/MM simulation of this site has been performed for a total of 6.5 ps. The orientation of the Met is preserved after an initial geometry optimization. However, after only 0.05 ps of dynamics, the binding site changes significantly, including a favorable orientation of the sulphur atom made possible by a torsional transition involving M138(Cγ). This indicates a relatively high efficiency of the dynamical scheme in relaxing the structure. The first 1.5 ps of the dynamics were carried out with the relatively small QM model previously described (23 atoms). It was observed that two classical oxygen atoms, one belonging to a solvent molecule (H_2Om), and one to the backbone of I139, came into axial positions, within bonding distance from the copper ion. Therefore the quantum system was increased to allow the metal to select freely between the two ligands. The extended system (36 QM atoms) involves a solvent molecule (H_2Om), and a part of the backbone, from Cα of I139 to C of H140. The subsequent evolution of the Cu-ligands distances is shown in Figure 2(a). During the dynamics, a rapid binding of the water molecule takes place, whereas the backbone oxygen drifts away, and stabilizes around 5 Å away from the copper ion. The dynamics was continued for 5 ps after the extension of the QM system, and a stable configuration was observed with H140(Nδ1), M138(S), D147(Oδ1), and D147(Oδ2) binding the copper ion in a roughly square planar geometry (torsional angle $T = 9(7)^\circ$) and a water molecule (H_2Om) in axial position. The bi-coordination of the copper ion by an aspartic acid is less frequent than mono-coordination, but is still present as ligand motif in the pool of protein analyzed (in 21% of the copper-aspartic acid contacts). The standard deviation of the Cu—H_2Om distance is the largest amongst all ligand distances, indicating that the axial position undergoes large fluctuations as can be expected. The RMSD of the QM region after equilibration with respect to the NMR structure is 2.3 Å, mainly due to a reorientation of the imidazole plane. The last frame of the dynamics is reported in Figure 2(b). Selected average distances are shown in Table II.

H140_D binding site

A second possible binding site was identified in proximity of H140, D144, and D147. The configuration at the end of the MM relaxation is distorted octahedral with the binding pocket formed by H140(Nε2), D144(Oδ2), D147 binding with both the carboxylic oxygen atoms, and two water molecules (H_2Oa and H_2Ob). Within roughly 3 ps of QM/MM dynamics the binding site undergoes a significant geometry reorganization. A chain of proton transfer reactions occurs from H_2Ob to H_2Oa and from H_2Oa to D147(Oδ1). Once neutralized, D147 drifts away from the metal centre and a further water molecule (H_2On) coordinates the metal in the axial position. The final binding site is trigonal bipyramidal with His(Nε2), D144(Oδ2), OH— in equatorial positions and two water molecules (H_2Ob, H_2On) settled in the two axial positions [Fig. 2(c)]. Copper coordination by three water molecules has been found rarely in the pool of proteins used for the statistical analysis. However, from the search for solvent exposed binding sites turned out that many of them are under-coordinated probably because some labile water ligands have not been resolved in the X-ray structures.

The same binding site was investigated after protonation of both of the imidazole nitrogen atoms to probe the features of a possible low pH form. Once protonated, the histidine side chain drifts away from the metal ion and the binding site rearranges to a distorted square planar geometry with a fifth axial ligand. Both the carboxylic oxygen atoms of D147 are involved in copper binding, together with the D144(Oδ2) and two water molecules (H140_DD binding site) [Fig. 2(d)].

DOI 10.1002/prot

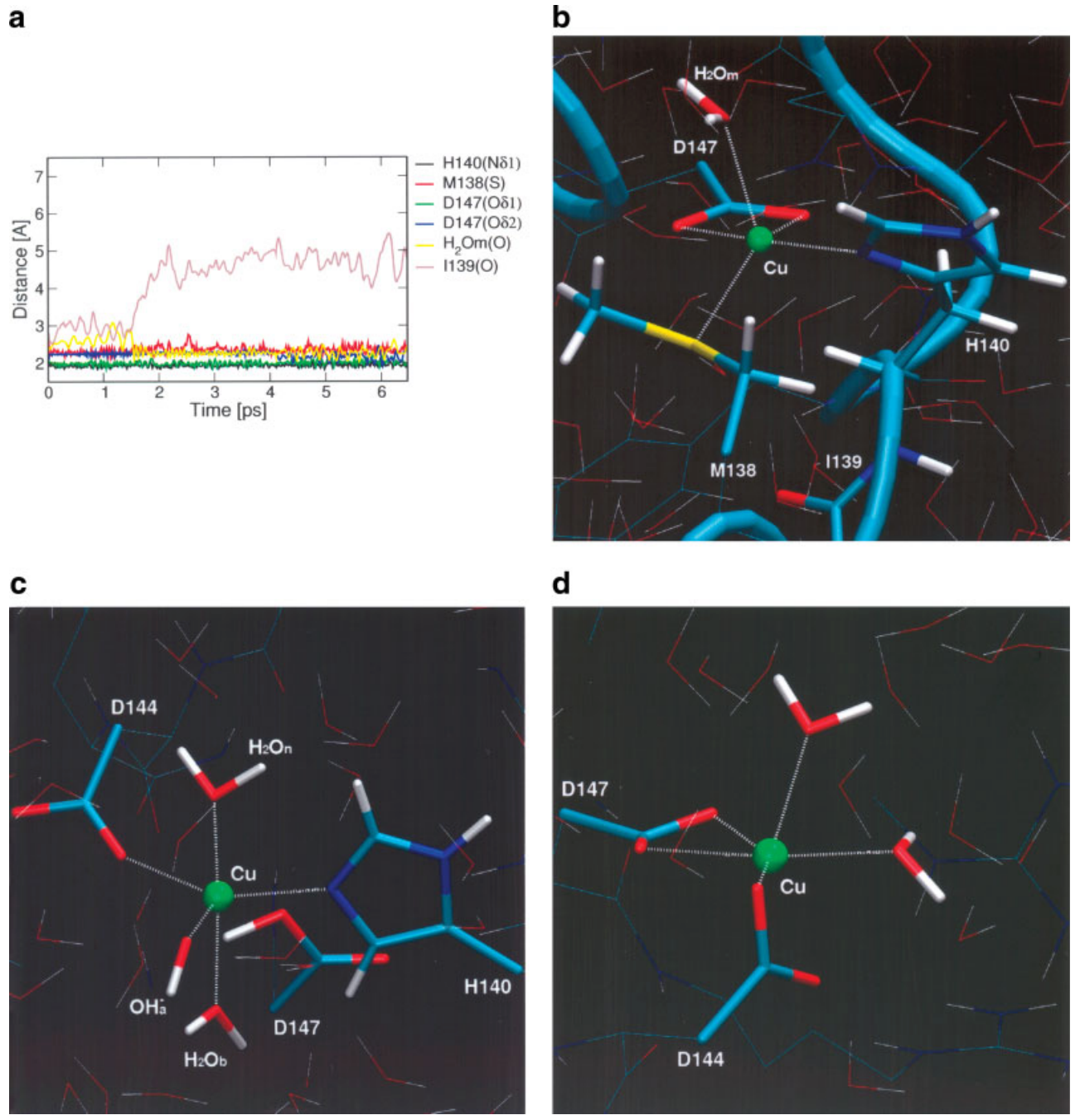

Figure 2

*(**a**) H140_M binding site. Evolution of the distances between Cu and its ligands along the QM/MM dynamics. Last snapshot of the QM/MM dynamics of the (**b**) H140_M binding site, (**c**) H140_D binding site, and (**d**) H140_DD binding site. Atoms in sticks are in the QM region.*

H177 binding site

This binding site is located at the N-terminus of HB (Fig. 1) and is highly solvent exposed. According to recent findings, the PrP^{c} to PrP^{Sc} transition should be accompanied by alterations in conformation of HB (50 apex).[50] The copper ion was placed on the surface of the protein among the side chains of H177 and D178 and four molecules of bulk water (H_2Oc, H_2Od, H_2Oe, H_2Of). The QM/MM dynamics was performed for 18.7 ps in total [Fig. 3(a)]. In the starting frame, obtained

Table II
Interatomic Distance Between Cu and Ligands in the H140_M, H177, H187_E, and H187_D Binding Site[a]

H140_M		H177		H187_E		H187_D	
H140(Nδ1)	1.94 (5)	H177(Nε2)	1.96 (6)	H187(Nε2)	2.06 (8)	H187(Nε2)	2.06 (7)
M138(S)	2.34 (7)	D178(Oδ1)	1.99 (8)	H_2Oh(O)	1.99 (6)	M206(S)	2.38 (9)
D147(Oδ1)	2.02 (7)	H_2Oc	2.01 (8)	E196(Oε2)	2.05 (7)	D202(Oδ2)	2.1 (1)
D147(Oδ2)	2.17 (9)	H_2Od	2.1 (1)	H_2Og(O)	1.99 (5)	H_2Oi(O)	2.1 (1)
H_2Om(O)	2.3 (1)	H_2Oe	2.3 (3)	T191(Oγ1)	2.3 (1)	H_2Oe(O)	2.1 (1)
I139(O)	4.7 (3)	H_2Of	5.5 (9)	R156(O)	4.2 (3)	R156(O)	6.0 (3)

[a]The average values and the standard error (in parentheses) are given in Å.

from the MM relaxation, all the residues forming the binding site are roughly at the same distance from the copper ion (between 2.15 and 2.50 Å) in an approximately octahedral geometry. During the QM/MM dynamics H_2Of drifts away from the copper ion and is eventually excluded from the quantum model. In a concerted mechanism, H177(Nε2), D178(Oδ1), and H_2Oc draw nearer to the copper binding it tightly, while H_2Od drifts towards the axial position and H_2Oe starts to oscillate above and below the plane formed by the equatorial ligands. During the last 3.5 ps of the simulation, H_2Oe settles in the equatorial plane [torsional angle $T = -9(9)$ defined by H177(Nε2), D178(Oδ1) H_2Oc(O), H_2Oe(O)], but with a larger average distance and standard deviation than the other ligands [Fig. 3(b)]. The rearrangement of the amino acids side chains due to Cu binding leads to an overall RMSD of the QM region of 0.98 Å. In the starting PDB structure both the D178 carboxylic oxygen atoms are involved in hydrogen bonds, one between D178(Oδ2) and Y128(Hη) and the other between D178(Oδ1) and R164(Hη11). At the end of the QM/MM simulation the hydrogen bond involving R164 was found to be broken and D178(Oδ1) binds to Cu(II), whereas the other hydrogen bond was preserved during all the dynamics. According to Daggett and coworkers,[46] the breaking of the latter hydrogen bond due to the neutralization of D178 at low pH is a possible trigger for the conversion from the PrP^c to PrP^{Sc} isoform.

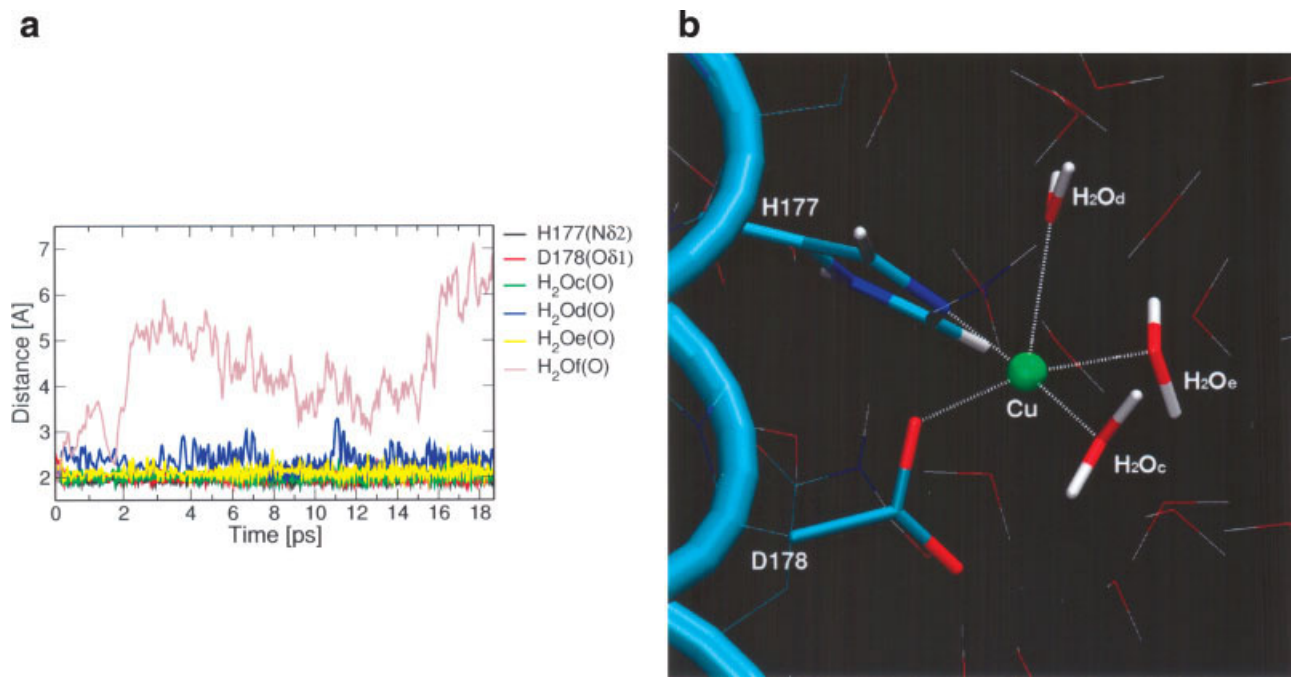

Figure 3
*(**a**) H177 binding site. Evolution of the distances between Cu and its ligands along the QM/MM dynamics. (**b**) H177 binding site. Last snapshot of the QM/MM dynamics. Atoms in sticks are in the QM region.*

DOI 10.1002/prot

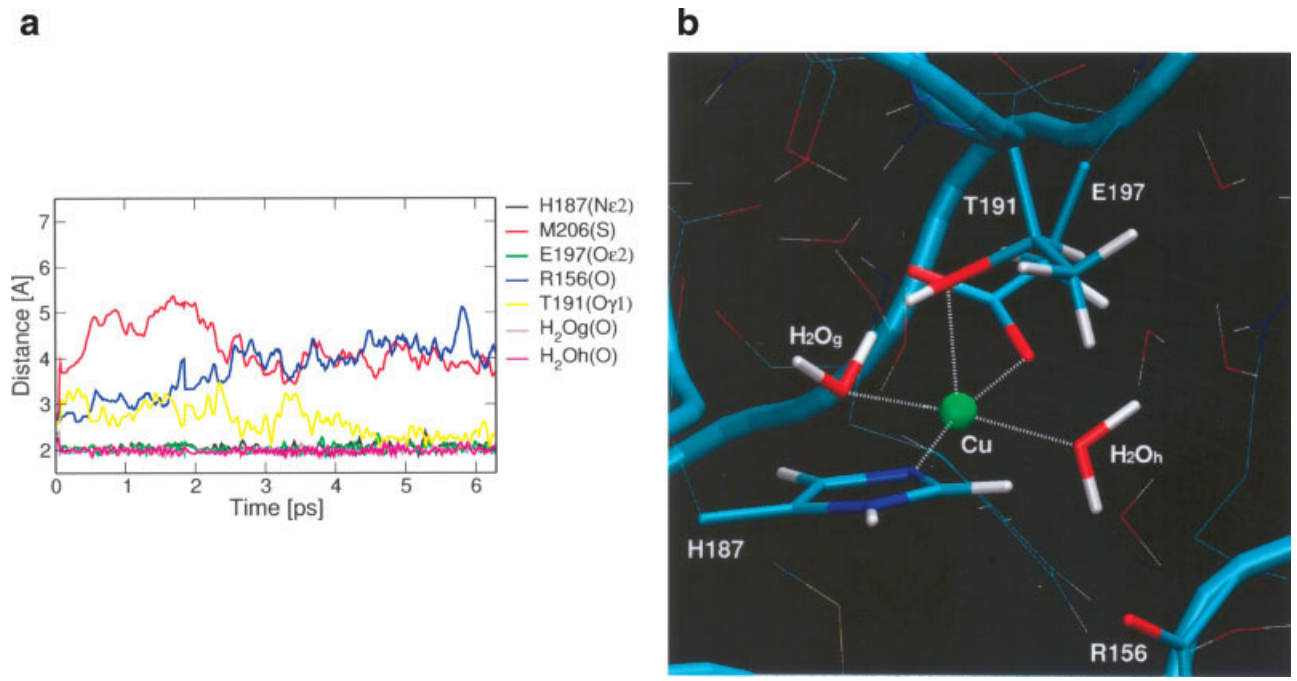

Figure 4

*(**a**) H187_E binding site. Evolution of the distances between Cu and its ligands along the QM/MM dynamics. (**b**) H187_E binding site. Last snapshot of the QM/MM dynamics. Atoms in sticks are in the QM region.*

H187_E binding site

This and the H187_D binding site involve the same His and are located at the border of the hydrophobic region, in the pocket formed by HA and HB towards the core of the protein (Fig. 1). His187, in particular is located in the second half of HB, a region that is hypothesized to undergo alteration in conformation during the misfolding process[50] and that should form β-strands according to secondary structure prediction studies.[77] In the starting geometry H187(Nε2), H_2Oh(O), E197(Oε2), E197(Oε1), H_2Og(O) are closer to the copper ion forming a distorted plane, whereas M206 and the backbone oxygen of R156 on one side and T191 on the other, are in competition for the axial positions. The QM/MM simulation has been performed for a total of 7 ps.

In the starting frame both E197(Oε1) and (Oε2) can possibly act as donors, their distance to Cu (II) being 2.59 and 2.39 Å, respectively. In addition, both lie in the plane of Cu, H187 and H_2Oh. After few steps of QM/MM dynamics E197(Oε1) starts to form a hydrogen bond with H_2Og moving away from the copper ion. Consequently, E197(Oε2) is free to bind to the copper ion and settles at a mean distance of 2.05 Å to the metal. The formation of the hydrogen bond between E197(Oε1) and H_2Og(H) triggers off the displacement of H_2Og towards the plane formed by H187(Nε2), H_2Oh(O), E197(Oε2) and its coordination to the copper at the average distance of 1.99 Å.

In the initial classical MD relaxation the sulphur atom of M206 and the backbone oxygen of R156 are fluctuating around the same distance to the copper ion. During the first 1.2 ps of QM/MM dynamics M206 moves away from the binding site and stabilizes around 4 Å away from the copper ion whereas the backbone oxygen of R156 stabilizes temporarily at bonding distance. Then R156(O) drifts slowly away from the metal towards H_2Oh, forming a hydrogen bond with this water molecule. As soon as R156(O) leaves the binding axial position, T191(Oγ1) approaches the copper stabilising at an average distance of 2.3(1) Å [Fig. 4(a)]. After roughly 3 ps of QM/MM dynamics the geometry of the binding site is defined, with H187(Nε2), H_2Oh(O), E197(Oε2), H_2Og(O) in a square planar geometry (torsional angle $T = -7(7)^\circ$), and T191(Oγ1) weakly bound in an axial position [Fig. 4(b)]. The dynamics was continued for 3 ps and this configuration remained stable. The RMSD of the QM binding site after equilibration compared with the metal free NMR structure is 1.7 Å, mainly due to the reorientation of the E196 side chain.

H187_D binding site

The initial geometry of the binding site consisted of seven ligands lying around the copper ion at distances spanning the range from 2.20 to 2.60 Å. In the initial geometry H187(Nε2), H_2Ol(O), D202(Oδ1), D202(Oδ2),

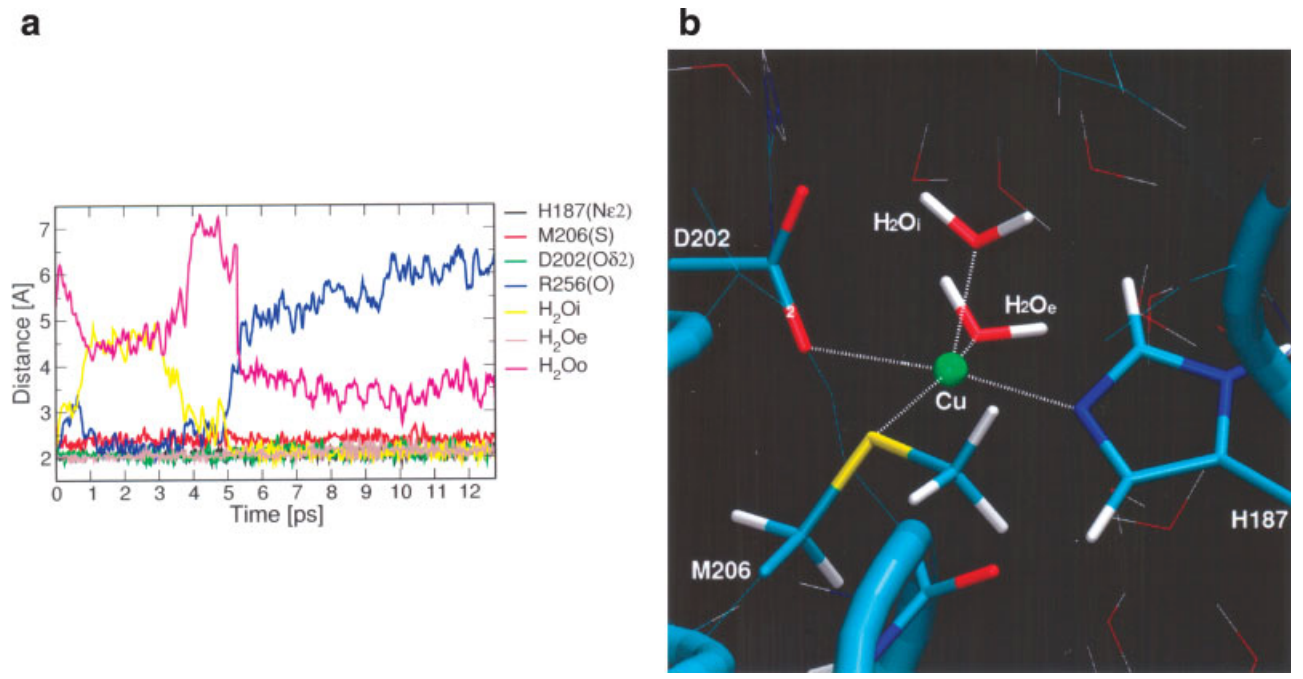

Figure 5

*(**a**) H187_D binding site. Evolution of the distances between Cu and its ligands along the QM/MM dynamics. (**b**) H187_D binding site. Last snapshot of the QM/MM dynamics. Atoms in sticks are in the QM region.*

R156(O) lie approximately in the same plane, with M206(S) and H_2Oi(O) in axial position. The QM/MM simulation was performed for a total of 12.8 ps. After 1 ps of QM/MM dynamics H_2Oi moves 4 Å away from Cu(II) with a classical water molecule replacing it in the ligands sphere. To allow the system to select between these two water molecules, the incoming classical molecule (H_2Oo) was also included into the quantum model. For the next 2 ps the two water molecules fluctuate around a distance of 4.2 Å from the copper ion before H_2Oo drifts away and H_2Oi draws nearer. In the meantime, D202(Oδ1) forms a hydrogen bond with H_2Oi and leaves the ligand sphere. Consequently, D202(Oδ2) is free to move closer to the copper stabilizing at 2.1(1) Å from it. Because of the insertion of H_2Oi between the metal and R156(O), the backbone drifts away [Fig. 5(a)]. At the end of this global rearrangement the geometry of the binding site is a distorted trigonal bipyramid with H187(Nε2) and D202(Oδ2) in the axial positions [Fig. 5(b)].

In summary, a total of six copper binding sites have been refined via QM/MM simulations. The H140_M, H177, and H187_E binding sites rearrange into square planar geometries, with a fifth weak ligand in axial position, whereas the H140_D, H187_D binding site form distorted trigonal bipyramids. The experimental EPR spectra of complex **2**[33] are typical for type-II protein-copper complexes, that are known to be largely square planar with a possible fifth ligand[78]; this excludes the H140_D and the H187_D binding sites as possible candidates for this complex. The H140_DD binding site, involving only aspartic acid residues and water molecules in the coordination pocket could be a representative candidate for complex **1**.[33]

All the candidate binding sites described in the text result in stable binding sites at least on the limited time scale of the first-principles QM/MM runs. As we cannot calculate directly the relative free energies of the putative binding sites, we have no theoretical means to determine the most stable site or the relative occupancy of the different candidate sites at room temperature. To make further contact with the data experimentally available, we use current state-of-art computational EPR methods to test the different structural models and to interpret experimental EPR data in a semi-quantitative way. To this end, we calculated the EPR characteristics of the three square planar binding sites characterized (H140_M, H177, and H187_E binding sites) and of the trigonal bipyramidal H187_D binding site.

EPR parameters calculation

Computation of Cu(II) A and g matrices

The spin Hamiltonian of a system with unpaired spins can be described in terms of the **g** matrix, the hyperfine

DOI 10.1002/prot

matrix **A** and the nuclear-quadrupole tensor **Q**. In case of Cu(II), the anisotropic component of the hyperfine matrix is not expected to be axial since there are contributions from all d orbitals. Nevertheless, in the experimental EPR spectra taken at the X-band, the resolution of the hyperfine splitting $A_{\perp}^{Cu}$ at $g_{\perp}$ is usually very low and consequently an average value is assumed for the spectral simulations. On the other hand, the hyperfine splitting at $g_{\|}$, $A_{\|}^{Cu}$, is usually much larger and clearly resolved in the experiments. Therefore, the comparison of the computational and experimental results mainly focuses on the $g_{\|}$ and $A_{\|}^{Cu}$ values. It has been previously suggested that $g_{\|}$ and $A_{\|}^{Cu}$ correlate with the type of donor atoms bound to Cu^{2+},[79] and some detailed diagrams have been compiled that link the type of ligands with $g_{\|}$ and $A_{\|}^{Cu}$ values.[80,81] However, the dependency of $g_{\|}$ and $A_{\|}^{Cu}$ values on the charge of the complex, leads to an overlap of some areas corresponding to different ligands, this sometimes prevents an univocal determination of the nature of the coordination sphere on the basis of the EPR data alone. Therefore, further tools must be invoked to unravel the atomistic details of the copper-binding sites.

Both the $A_{\|}^{Cu}$ and the **g** matrix components calculated with the approach outlined here are reported in Tables III and IV, respectively, together with the experimental values for complex **2** (pH 3–8).[32,33]

The hyperfine coupling matrix (**A** matrix) has two contributions: the isotropic, or Fermi, component (a_{iso}), and the anisotropic, or dipolar, component ($\mathbf{A_D}$ matrix).

The spin polarization effect is of major importance in the computation of a_{iso},[82,83] since this parameter is related to the spin density at the magnetic nucleus. However, in some cases the contribution of this effect to the $\mathbf{A_D}$ matrix is also non negligible.[82,84,85] The spin-orbit interaction is known to contribute significantly to both components of the hyperfine coupling for transition metals,[86,87] and to play a special role in the determination of the $\mathbf{A_D}$ matrix.[69,86,87,88] Therefore, the most accurate approach would be to take into account the spin-polarization effects in the spin orbit coupled equations,[89] but this is not possible in the ADF2002.01 software package. Thus, in order to have the most accurate **A** matrix values for transition metals for which spin-orbit effects are important, we adopted the protocol suggested by Saladino and Larsen[69] and described in the "Methods" section of the present paper, that is, using a mixture of spin polarized (**g** and the $\mathbf{A_D}$ matrices) and spin unpolarized (a_{iso}) calculations. Such a procedure can be viewed with some concern as the two components of the **A** matrix are not treated at a consistent level of theory and should be evaluated separately. However it turns out that this approximation is not the major source of error, since the accuracy is predominantly limited by the density functionals presently available.[83] Currently available exchange-correlation functionals are in fact not able to give uniformly satisfactory agreement with experiments for the **g** and **A** matrix for transition metals atoms, no matter which level of theory is used to compute the EPR parameters.[90] Therefore, we focus here on a semi-quantitative comparison with the experimental data. As shown in previous studies,[88,91,92] the protocol we adopted here is able to reproduce semi-quantitatively the experimental hyperfine coupling constants and to follow the experimental trends of a series of Cu(II) and VO^{2+} complexes.

Table III
Computed and Experimental g Matrix[a]

Binding site	g_{zz} ($g_{\|}$)	g_{yy}	g_{xx}	$g_{\perp}$
H140_M	2.138 (2)	2.052 (2)	2.024 (2)	2.038 (3)
H177	2.17 (1)	2.065 (7)	2.01 (1)	2.037 (9)
H187_E	2.191 (5)	2.062 (5)	2.040 (2)	2.051 (4)
H187_D	2.149 (4)	2.094 (5)	2.026 (8)	2.060 (9)
exp.(32, 33)	2.295 ± 0.005			2.068 ± 0.005
PrP(180-193) (35)	2.250			

[a]The statistical error due to thermal fluctuation is given in parentheses.

From Table III, one can see that the $A_{\|}^{Cu}$ values of both the H177 and the H187_E binding sites are in agreement with the experiments whereas the binding sites including Met as a ligand (H140-M and H187_D) are excluded. Unfortunately, the $A_{\|}^{Cu}$ values of the H177 and H187_E binding sites are equal within the statistical error due to thermal fluctuation since they contain the same metal-coordinating atoms. In this situation, the $A_{\|}^{Cu}$ parameter is not sufficient to discriminate between them.

The **g** matrix is computed with the SO+SR ROKS approach, since the spin orbit coupling is recognized to be the most important factor for the determination of g values.

The g_{xx} and g_{yy} components of the computed **g** matrix for the square planar complexes have similar values and are smaller then g_{zz} ($g_{\|}$ in the experiments). This is in agreement with the experimental trend[32,33] where the resolution of these components is low and an average value, $g_{\perp}$, is assumed. This is also expected for a Type-II copper protein.[78] Furthermore, the computations clearly show that the involvement of a sulphur atom in the binding site reduces $g_{\|}$ considerably, confirming the empirical trend reported in Ref. 81.

However, the computed $g_{\|}$ seems to be underestimated when compared with the diagrams compiled by Peisach and Blumberg.[81] The same tendency has been reported by other authors working with a density functional approach on systems containing elements heavier than the ones in the first- and second-row.[93–98] In particular, Saladino and Larsen computed the EPR parameters for a series of four square planar Cu(II)-complexes using the same code and protocol we used here.[69] An underestimation of the computed $g_{\|}$ value ranging between 87 and 200 ppt is observed for all of them. The nitrogen-containing Cu(II)-binding sites have lower $g_{\|}$ values

Table IV
Computed and Experimental Hyperfine Interaction for the Copper Atom[a]

Binding site	$A_{zz}^{Cu}(A_{\|})$
H140_M	−351 (47)
H177	−470 (10)
H187_E	−465 (21)
H187_D	−393 (8)
exp(32, 33)	$\|457\| \pm 10$
PrP(180–193) (35)	$\|516\|$

[a]The average values and the statistical error due to thermal fluctuation (in parentheses) are given in MHz.

compared with the oxygen containing ones and the decrease is more intense for system with higher charge delocalization, in agreement with experimental trends.[81]

The experimental $g_{\|}$ (2.295 ± 0.005) (Table IV) falls in the range of values associated to the binding sites involving nitrogen and oxygen as ligands, but excludes sulphur.[81] This speaks against the involvement of sulphur atoms in the first coordination sphere as was also found by means of the computed $A_{\|}^{Cu}$ parameter. Keeping in mind the systematic underestimation of the **g** matrix mentioned above, also the $g_{\|}$ parameter point to this conclusion. Therefore, according to the calculated $A_{\|}^{Cu}$ and **g** matrix the two most likely candidates for the experimentally observed complex **2** are the H177 and H187_E binding sites. However nor $A_{\|}^{Cu}$ nor $g_{\|}$ is sufficient to discriminate between this two binding sites and additional parameters such as the hyperfine constants of the ligand atoms, have been considered.

Computation of the hyperfine matrix for the surrounding N nuclei

Besides the hyperfine interaction with the copper nucleus, the unpaired electron also couples to the surrounding nuclei with non-zero nuclear magnetic moment. These hyperfine interactions can be studied experimentally with different EPR techniques, such as ESEEM and ENDOR.

Table V shows the computed isotropic hyperfine coupling constant a_{iso} for the copper coordinating imidazole nitrogen atom. The best agreement is obtained for H140_M binding site. However, since the theoretical error for this quantity in Cu-histidine complexes is estimated to be ±5 MHz,[70] both models H_140_M and H187_E are in agreement with the experimental value. H140_M can be excluded on the base of $A_{\|}^{Cu}$ (Table III) and H187_E remains the most likely candidate that does not violate the experimental EPR parameters.

However, the H187_E binding site contradicts the experimental data on one point, namely the involvement of water in the metal-coordination sphere [Fig. 4(b)]. Although proton hyperfine couplings matching those found for Cu(II) complexes with equatorial water coordination were observed in the ENDOR and HYSCORE spectra of complex **2**, the ENDOR spectra of Cu(II)-bound mPrP(23–231) in D_2O seemed to indicate that the observed protons were non-exchangeable and therefore not due to water ligation.[33] However, as shown in detail later, re-evaluation of these ENDOR data in combination with HYSCORE spectra of the Cu(II)-bound mPrP(23–231) in D_2O indicates that partial exchange of the protons does occur, which agree with the coordination sphere observed for the H187_E binding site. The involvement of H187 in the coordination of Cu(II) is also experimentally supported by the EPR and CD study of copper-binding to different prion mutants[34] and by the fact that the EPR parameters of complex **2**[33] are in good agreement with those observed for a Cu(II)-PrP Ac180-193NH2 complex[40] (Table IV) suggesting H187 as the most likely experimentally observed binding site.

According to some experimental findings, the C-terminal part of PrP is capable of propagating prion disease.[99,100] In particular, the reversible inactivation of the PrP^{Sc} after proteinase K digestion by means of diethyl pyrocarbonate (DEP)[101] points to a central role played by C-terminal histidine residues in the infection process. Furthermore, the H187R mutation[102] is the only known variant involving histidine residues inducing familial encephalopathy. It has been pointed out that HB, along which H187 is located, is likely to have a role in the nucleation process and fibrillization of the PrP^{Sc}.[103,104] In particular, according to NMR experiments[105,106] and a combination of sequence pattern matches and MD simulations,[50] the C-terminal part of the HB is indicated as playing a central role in the transition from the cellular to the pathogenic PrP isoform. All these findings together support the importance of H187 and the HB region in the understanding of the PrP^{c} to PrP^{Sc} structural transition.

Reinterpretation of the proton couplings in Cu(II)-bound mPrP(23–321) at pH 3–8

In Ref. 33, the Davies-ENDOR spectra of Cu(II)-bound mPrP(23–321) in H_2O and D_2O were compared. This experiment showed that the peaks related to the strongest proton interaction (splitting of 8 MHz at the

Table V
Computed and Experimental A Matrix for the Imidazole Cu-Coordinating Nitrogen Atom[a]

Binding site		a_{iso}
H140_M	Nδ1	27 (1)
H177	Nε2	38 (1)
H187_E	Nε2	31 (1)
H187_D	Nε2	35 (1)
exp. (33)		26 (1)

[a]The average values and the statistical error due to thermal fluctuation (in parentheses) are given in MHz. The prime apex indicates the usage of a local set of axes different than the one used for the copper hyperfine matrix.

DOI 10.1002/prot

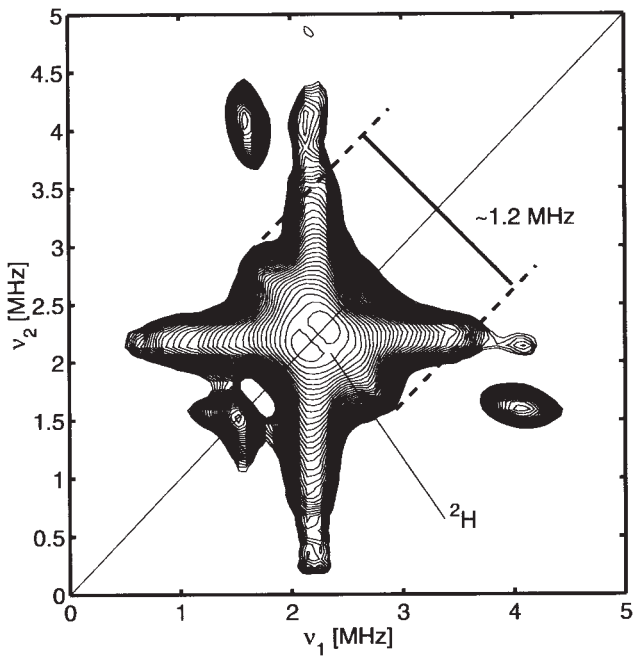

Figure 6

Experimental HYSCORE spectrum of Cu(II)-bound mPrP(23–231) at observer position C [see position marked in Fig. 1(a) of Ref. 33]. The experimental conditions for the HYSCORE recording and protein preparations are identical as given in the latter reference.

observer position $g_\perp$) were still clearly present in the D_2O samples. The obvious conclusion was that this interaction can be ascribed to a non-exchangeable proton and, despite the similarities with proton hyperfine couplings of equatorially coordinated water, can not be due to water ligands.

However, in the light of the present theoretical findings, we decided to reconsider the previous experimental data. For the sake of clarity, we will call the signals related to the strongest proton interaction, H1. It is definitely undisputable, that the H1 signal is still observable in the ENDOR spectra after addition of D_2O [see Fig. 4C of Ref. 33], so that total exchange can be excluded. However, since we have no internal reference signal in the ENDOR spectra and since the spectral intensity depends on several factors (protein concentration, microwave pulse setting, filling factor of the cavity, etc.), it is impossible to determine from these spectra, whether the H1 signal intensity has not decreased to some extend with respect to the non-deuterated case.

HYSCORE experiments can provide us with such a reference point, namely the double-quantum cross-peaks related to the nitrogen interactions. If the H1 signal, which can clearly be observed in the HYSCORE spectra [see Fig. 5(a) of Ref. 33], remains unaffected by the deuteration of water, then the ratio of the cross-peaks intensities of the H1 signal versus the nitrogen cross-peaks should remain unchanged. This turns out not to be the case. The intensity of the H1 signal decreases by a factor of ~4.5 with respect to the nitrogen peak intensities, indicating that partial exchange has occurred. Furthermore, additional proof of a partial exchange comes from the study of the cross-peaks in the deuterium region (Fig. 6). The majority of the deuterium signal stems from the more distant deuterons (leading to a sharp cross-peak on the diagonal situated at the nuclear Zeeman frequency of ^{2}H). However, upon lowering the contour lines, a maximum width of 1.2 MHz is observed. In the proton HYSCORE spectra the maximum observed width is about 8 MHz [see Fig. 5(a) of Ref. 33] and $8*g_n$ (^{2}H)/g_n (^{1}H) is 1.22 MHz. Furthermore, the ^{2}H nuclear-quadrupole interaction is known to be small. In Figure 7, a simulated HYSCORE spectrum is shown for an interaction with a ^{2}H nucleus assuming $\mathbf{A}$ = [1.22, −1.22, −1.22] MHz [obtained from scaling the proton hyperfine values by multiplying with g_n (^{2}H)/g_n (^{1}H)] and a typical ^{2}H nuclear-quadrupole interaction ($|e2qQ/h|$ = 0.26 MHz and η = 0.5). One can clearly see that the maximal width of experimental spectrum is reproduced. Note, that in the experiment, the intensity on the diagonal is larger, due to the contributions of distant deuterons. The cross-peaks at (1.5, 4) MHz and (1.5, 1.5) MHz stem from the nitrogen interactions [see also Fig. 2(a), Ref. 33].

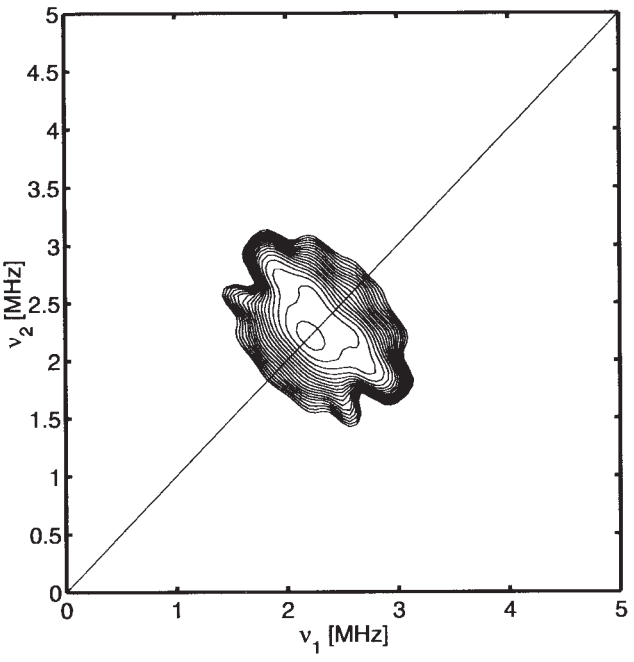

Figure 7

Simulation of the 2H contribution to the HYSCORE spectrum in Figure 6 using the parameters mentioned in the text.

The earlier points clearly show that the protons related to the H1 signal are (partially) exchangeable. The question is then whether the relative low decrease in intensity (factor 4.5) matches the deuteration conditions? First of all, since non-deuterated glycerol was used as a cryoprotectant, this will easily increase the rest-amount of H_2O to percentages around 10%. Furthermore, although the EPR spectrum is dominated by contributions of complex **2**, there is still a small fraction of complex **1** left at this pH range. This complex may have non-exchangeable protons with strong couplings, which may underlie the spectrum of complex **1** and which will diminish the apparent reduction of the H1 signal intensity. Finally, exchange with water from the air may have occurred, reducing the degree of deuteration. All these factors may well add up to the relatively low exchange of about 75 % that is observed.

SUMMARY AND CONCLUSIONS

We identified putative copper binding sites in the C-terminal domain of the mouse PrP by means of a statistical analysis of copper coordination in known protein structures. The detailed structural features of all binding sites were subsequently refined via hybrid QM/MM molecular dynamics simulations. Three of the sites involving histidine (H140_M, H177, H187_E binding sites) rearrange to a square planar geometry with a fifth weak ligand, in agreement with the information obtained by the experimental EPR data for the complex **2** at pH 3–8. The comparison of the experimental and computed EPR parameters, together with the reinterpretation of the experimental proton coupling in the light of the theoretical results and the study of the state-of-the-art knowledge of the metal binding to PrP, allows to narrow down the likely candidates to the H187_E binding site, involving H187, E196, T191, and two water molecules. A further binding site (H140_DD binding site) was identified as a possible candidate for the experimental complex **1** at low pH. The atomistic details we provided can now be probed experimentally in order to further refine the location of the copper ion in the PrP and give possible insights into the structural function of the metal ion in this protein.

ACKNOWLEDGMENTS

We thank the Swiss National Supercomputing Centre (CSCS) for the computer time provided and we are grateful to Dr. Alessandro Ponti for helpful discussions.

REFERENCES

1. Prusiner SB. Prions. Proc Natl Acad Sci USA 1998;95:13363–13383.
2. Riek R, Hornemann S, Wider G, Billeter M, Glockshuber R, Wuthrich K. NMR structure of the mouse prion protein domain PrP(121-231). Nature 1996;382:180–182.
3. Liu H, Farr-Jones S, Ulyanov NB, Llinas M, Marqusee S, Groth D, Cohen FE, Prusiner SB, James TL. Solution structure of Syrian hamster prion protein rPrP(90-231). Biochemistry 1999;38:5362–5377.
4. Knaus KJ, Morillas M, Swietnicki W, Malone M, Surewicz WK, Yee VC. Crystal structure of the human prion protein reveals a mechanism for oligomerization. Nat Struct Biol 2001;8:770–774.
5. Haire LF, Whyte SM, Vasisht N, Gill AC, Verma C, Dodson EJ, Dodson GG, Bayley PM. The crystal structure of the globular domain of sheep prion protein. J Mol Biol 2004;336:1175–1183.
6. Brown DR, Qin KF, Herms JW, Madlung A, Manson J, Strome R, Fraser PE, Kruck T, von Bohlen A, SchulzSchaeffer W, Giese A, Westaway D, Kretzschmar H. The cellular prion protein binds copper in vivo. Nature 1997;390:684–687.
7. Brown DR. Metallic prions. Biochem Soc Symp 2004;71:193–202.
8. Brown DR, Kozlowski H. Biological inorganic and bioinorganic chemistry of neurodegeneration based on prion and Alzheimer diseases. Dalton Trans 2004;13:1907–1917.
9. Vassallo N, Herms J. Cellular prion protein function in copper homeostasis and redox signalling at the synapse. J Neurochem 2003;86:538–544.
10. Lehmann S. Metal ions and prion diseases. Curr Opin Chem Biol 2002;6:187–192.
11. Viles JH, Cohen FE, Prusiner SB, Goodin DB, Wright PE, Dyson HJ. Copper binding to the prion protein: structural implications of four identical cooperative binding sites. Proc Natl Acad Sci USA 1999;96:2042–2047.
12. Rachidi W, Vilette D, Guiraud P, Arlotto M, Riondel J, Laude H, Lehmann S, Favier A. Expression of prion protein increases cellular copper binding and antioxidant enzyme activities but not copper delivery. J Biol Chem 2003;278:9064–9072.
13. Hornshaw MP, McDermott JR, Candy JM. Copper binding to the N-terminal tandem repeat regions of mammalian and avian prion protein. Biochem Biophys Res Commun 1995;207:621–629.
14. Jackson GS, Murray I, Hosszu LLP, Gibbs N, Waltho JP, Clarke AR, Collinge J. Location and properties of metal-binding sites on the human prion protein. Proc Natl Acad Sci USA 2001;98:8531–8535.
15. Pauly PC, Harris DA. Copper stimulates endocytosis of the prion protein. J Biol Chem 1998;273:33107–33110.
16. Whittal RM, Ball HL, Cohen FE, Burlingame AL, Prusiner SB, Baldwin MA. Copper binding to octarepeat peptides of the prion protein monitored by mass spectrometry. Protein Sci 2000;9:332–343.
17. Burns CS, Aronoff-Spencer E, Dunham CM, Lario P, Avdievich NI, Antholine WE, Olmstead MM, Vrielink A, Gerfen GJ, Peisach J, Scott WG, Millhauser GL. Molecular features of the copper binding sites in the octarepeat domain of the prion protein. Biochemistry 2002;41:3991–4001.
18. Shiraishi N, Ohta Y, Nishikimi M. The octapeptide repeat region of prion protein binds Cu(II) in the redox-inactive state. Biochem Biophys Res Commun 2000;267:398–402.
19. Brown DR, Wong BS, Hafiz F, Clive C, Haswell SJ, Jones IM. Normal prion protein has an activity like that of superoxide dismutase. Biochem J 1999;344:1–5.
20. Wong BS, Pan T, Liu T, Li RL, Gambetti P, Sy MS. Differential contribution of superoxide dismutase activity by prion protein in vivo. Biochem Biophys Res Commun 2000;273:136–139.
21. Cui T, Daniels M, Wong BS, Li RL, Sy MS, Sassoon J, Brown DR. Mapping the functional domain of the prion protein. Eur J Biochem 2003;270:3368–3376.
22. Sakudo A, Lee DC, Nishimura T, Li SM, Tsuji S, Nakamura T, Matsumoto Y, Saeki K, Itohara S, Ikuta K, Onodera T. Octapeptide repeat region and N-terminal half of hydrophobic region of prion protein (PrP) mediate PrP-dependent activation of superoxide dismutase. Biochem Biophys Res Commun 2005;326:600–606.
23. Hutter G, Heppner FL, Aguzzi A. No superoxide dismutase activity of cellular prion protein in vivo. Biol Chem 2003;384:1279–1285.

 DOI 10.1002/prot

24. Sakudo A, Hamaishi M, Hosokawa-Kanai T, Tuchiya K, Nishimura T, Saeki K, Matsumoto ,Y, Ueda S, Onodera T. Absence of superoxide dismutase activity in a soluble cellular isoform of prion protein produced by baculovirus expression system. Biochem Biophys Res Commun 2003;307:678–683.
25. Aronoff-Spencer E, Burns CS, Avdievich NI, Gerfen GJ, Peisach J, Antholine WE, Ball HL, Cohen FE, Prusiner SB, Millhauser GL. Identification of the Cu^{2+} binding sites in the N-terminal domain of the prion protein by EPR and CD spectroscopy. Biochemistry 2000;39:13760–13771.
26. Burns CS, Aronoff-Spencer E, Legname G, Prusiner SB, Antholine WE, Gerfen GJ, Peisach J, Millhauser GL. Copper coordination in the full-length, recombinant prion protein. Biochemistry 2003;42: 6794–6803.
27. Burns CS, Aronoff-Spencer E, Dunham CM, Lario P, Avdievich NI, Antholine WE, Olmstead MM, Vrielink A, Gerfen GJ, Peisach J, Scott WG, Millhauser GL. Molecular features of the copper binding sites in the octarepeat domain of the prion protein. Biochemistry 2002;41:3991–4001.
28. Miura T, Hori-IA, Mototani H,Takeuchi H. Raman spectroscopic study on the copper(II) binding mode of prion octapeptide and its pH dependence. Biochemistry 1999;38:11560–11569.
29. Garnett AP, Viles JH. Copper binding to the octarepeats of the prion protein—affinity, specificity, folding, and cooperativity: insights from circular dichroism. J Biol Chem 2003;278:6795–6802.
30. Kramer ML, Kratzin HD, Schmidt B, Romer A, Windl O, Liemann S, Hornemann S, Kretzschmar H. Prion protein binds copper within the physiological concentration range. J Biol Chem 2001; 276:16711–16719.
31. Morante S, González-Iglesias R, Potrich C, Meneghini C, Meyer-Klaucke W, Menestrina G, Gasset M. Inter- and intra-octarepeat Cu(II) site geometries in the prion protein. J Biol Chem 2004;279: 11753–11759.
32. Cereghetti GM, Schweiger A, Glockshuber R, Van Doorslaer S. Electron paramagnetic resonance evidence far binding of Cu^{2+} to the C-terminal domain of the murine prion protein. Biophys J 2001;81:516–525.
33. Van Doorslaer S, Cereghetti GM, Glockshuber R, Schweiger A. Unraveling the Cu^{2+} binding sites in the C-terminal domain of the murine prion protein: a pulse EPR and ENDOR study. J Phys Chem B 2001;105:1631–1639.
34. Cereghetti GM, Schweiger A, Glockshuber R, Van Doorslaer S. Stability and Cu(II) binding of prion protein variants related to inherited human prion diseases. Biophys J 2003;84:1985–1997.
35. Brown DR, Guantieri V, Grasso G, Impellizzeri G, Pappalardo G, Rizzarelli E. Copper(II) complexes of peptide fragments of the prion protein. Conformation changes induced by copper(II) and the binding motif in C-terminal protein region. J Inorg Biochem 2004;98:133–143.
36. Hasnain SS, Murphy LM, Strange RW, Grossmann JG, Clarke AR, Jackson GS, Collinge J. XAFS study of the high-affinity copper-binding site of human PrP91-231 and its low-resolution structure in solution. J Mol Biol 2001;311:467–473.
37. Stockel J, Safar J, Wallace AC, Cohen FE, Prusiner SB. Prion protein selectively binds copper(II) ions. Biochemistry 1998;37:7185–7193.
38. Flechsig E, Shmerling D, Hegyi I, Raeber AJ, Fischer M, Cozzio A, von Mering C, Aguzzi A, Weissmann C. Prion protein devoid of the octapeptide repeat region restores susceptibility to scrapie in PrP knockout mice. Neuron 2000;27:399–408.
39. Wong BS, Chen SG, Colucci M, Xie ZL, Pan T, Liu T, Li RL, Gambetti P, Sy MS, Brown DR. Aberrant metal binding by prion protein in human prion disease. J Neurochem 2001;78:1400–1408.
40. Rachidi W, Mange A, Senator A, Guiraud P, Riondel J, Benboubetra M, Favier A, Lehmann S. Prion infection impairs copper binding of cultured cells. J Biol Chem 2003;278:14595–14598.
41. Sigurdsson EM, Brown DR, Alim MA, Scholtzova H, Carp R, Meeker HC, Prelli F, Frangione B, Wisniewski T. Copper chelation delays the onset of prion disease. J Biol Chem 2003;278:46199–46202.
42. Requena JR, Groth D, Legname G, Stadtman ER, Prusiner SB, Levine RL. Copper-catalyzed oxidation of the recombinant SHa(29-231) prion protein. Proc Natl Acad Sci USA 2001;98:7170–7175.
43. Giese A, Levin J, Bertsch U, Kretzschmar H. Effect of metal ions on de novo aggregation of full-length prion protein. Biochem Biophys Res Commun 2004;320:1240–1246.
44. Okimoto N, Yamanaka K, Suenaga A, Hata M, Hoshino T. Computational studies on prion proteins: effect of Ala(117) -> val mutation. Biophys J 2002;82:2746–2757.
45. El-Bastawissy E, Knaggs MH, Gilbert IH. Molecular dynamics simulations of wild-type and point mutation human prion protein at normal and elevated temperature. J Mol Graph Model 2001;20: 145–154.
46. Alonso DOV, DeArmond SJ, Cohen FE, Daggett V. Mapping the early steps in the pH-induced conformational conversion of the prion protein. Proc Natl Acad Sci USA 2001;98:2985–2989.
47. Parchment OG, Essex JW. Molecular dynamics of mouse and syrian hamster PrP: implications for activity. Proteins 2000;38:327–340.
48. Zuegg J, Gready JE. Molecular dynamics simulations of human prion protein: importance of correct treatment of electrostatic interactions. Biochemistry 1999;38:13862–13876.
49. Ji HF, Zhang HY, Shen LA. The role of electrostatic interaction in triggering the unraveling of stable helix 1 in normal prion protein. A molecular dynamics simulation investigation. J Biomol Struct Dyn 2005;22:563–570.
50. Dima RI, Thirumalai D. Probing the instabilities in the dynamics of helical fragments from mouse PrPc. Proc Natl Acad Sci USA 2004;101:15335–15340.
51. Karplus M, Petsko GA. Molecular-dynamics simulation in biology. Nature 1990;347:631–639.
52. Laio A, VandeVondele J, Rothlisberger U. A Hamiltonian electrostatic coupling scheme for hybrid Car-Parrinello molecular dynamics simulations. J Chem Phys 2002;116:6941–6947.
53. Dal Peraro M, Llarrull LI, Rothlisberger U, Vila AJ, Carloni P. Water-assisted reaction mechanism of monozinc β-lactamases. J Am Chem Soc 2004;126:12661–12668.
54. Guidoni L, Spiegel K, Zumstein M, Rothlisberger U. Green oxidation catalysts: computational design of high-efficiency models of galactose oxidase. Angew Chem Int Ed Engl 2004;43:3286–3289.
55. Spiegel K, Rothlisberger U, Carloni P. Cisplatin binding to DNA oligomers from hybrid Car-Parrinello/molecular dynamics simulations. J Phys Chem B 2004;108:2699–2707.
56. van Gunsteren WF, Billeter SR, Eising AA, Hünenberger PH, Krüger PKHC, Mark AE, Scott WRP, Tironi IG. Biomolecular simulation: the GROMOS96 manual and user guide. Zürich: vdf Hochschulverlag AG; 1996.
57. te Velde G, Bickelhaupt FM, van Gisbergen SJA, Fonseca Guerra C, Baerends EJ, Snijders JG, Ziegler T. Chemistry with ADF. J Comput Chem 2001;22:931–967.
58. Guerra CF, Snijders JG, te Velde G, Baerends EJ. Towards an order-N DFT method. Theor Chem Acc 1998;99:391–403.
59. ADF2002.01, SCM. Theoretical chemistry. Vrije Universiteit, Amsterdam, The Netherlands. http://www.scm.com.
60. Dolittle RF. Redundancies in protein sequences. In: Fasman GD, editor. Prediction of protein structure and the principles of protein conformation. New York: Plenum; 1989. pp 599–623.
61. Hünenberger PH. Optimal charge-shaping functions for the particle-particle-particle-mesh (P3M) method for computing electrostatic interactions in molecular simulations. J Chem Phys 2000; 113:10464–10476.
62. Becke AD. Density-functional exchange-energy approximation with correct asymptotic behaviour. Phys Rev A 1988;38:3098–3100.
63. Lee CT, Yang WT, Parr RG. Development of the Colle-Salvetti correlation-energy formula into a functional of the electron density. Phys Rev B 1988;37:785–789.

64. Troullier N, Martins JL. Efficient pseudopotentials for plane wave calculations. Phys Rev B 1991;43:1993–2006.
65. Martyna GJ, Tuckerman ME. A reciprocal space based method for treating long range interactions in ab initio and force-field-based calculations in clusters. J Chem Phys 1999;110:2810–2821.
66. Laio A, Gervasio FL, VandeVondele J, Sulpizi M, Rothlisberger U. A variational definition of electrostatic potential derived charges. J Phys Chem B 2004;108:7963–7968.
67. van Lenthe E, Wormer PES, van der Avoird A. Density functional calculations of molecular *g*-tensors in the zero-order regular approximation for relativistic effects. J Chem Phys 1997;107:2488–2498.
68. van Lenthe E, van der Avoird A, Wormer PES. Density functional calculations of molecular hyperfine interactions in the zero order regular approximation for relativistic effects. J Chem Phys 1998; 108:4783–4796.
69. Saladino AC, Larsen SC. Relativistic DFT calculations of copper hyperfine coupling constants: effect of spin-orbit coupling. J Phys Chem A 2003;107:5583–5587.
70. Baute D, Arieli D, Neese F, Zimmermann H, Weckhuysen BM, Goldfarb D. Carboxylate binding in copper histidine complexes in solution and in zeolite Y: X- and W-band pulsed EPR/ENDOR combined with DFT calculations. J Am Chem Soc 2004;126: 11733–11745.
71. Naumov S, Reinhold J, Beckert D. Investigation of the molecular structure of the radical anions of some pyrimidine-type bases in aqueous solution by comparison of calculated hyperfine coupling constants with EPR results. Phys Chem Chem Phys 2003;5:64–72.
72. Vosko SH, Wilk L, Nusair M. Accurate spin dependent electron liquid correlation energies for local spin-densities calculations—a critical analysis. Can J Phys 1980;58:1200–1211.
73. Perdew JP. Density functional approximation for the correlation-energy of the inhomogeneous electon-gas. Phys Rev B 1986;33: 8822–8824.
74. van Lenthe E, Baerends EJ, Snijders JG. Relativistic regular two-component Hamiltonians. J Chem Phys 1993;99:4597–4610.
75. van Lenthe E, Baerends EJ, Snijders JG. Relativistic total energy using regular approximations. J Chem Phys 1994;101:9783–9792.
76. van Lenthe E, Ehlers A, Baerends EJ. Geometry optimizations in the zero order regular approximation for relativistic effects. J Chem Phys 1999;110:8943–8953.
77. Kallberg Y, Gustafsson M, Persson B, Thyberg J, Johansson J. Prediction of amyloid fibril-forming proteins J Biol Chem 2001;276: 12945–12950.
78. Messerschmidt A. Metal sites in small blue copper proteins, blue copper oxidases and vanadium-containing enzymes. Struct Bonding 1998;90:37–68.
79. Kivelson D, Neiman R. ESR studies on bonding in copper complexes. J Chem Phys 1961;35:149–155.
80. Vänngärd T. Copper proteins. In: Swartz HM, Bolton JR, Borg DC, editors. Biological applications of electron spin resonance. New York: Wiley-Interscience; 1972. pp 411–447.
81. Peisach J, Blumberg WE. Structural implications derived from the analysis of electron paramagnetic resonance spectra of natural and artificial copper proteins. Arch Biochem Biophys 1974;165:961–708.
82. Munzarova ML, Kaupp M. A density functional study of EPR parameters for vanadyl complexes containing Schiff base ligands. J Phys Chem B 2001;105:12644–12652.
83. Neese F. Metal and ligand hyperfine couplings in transition metal complexes: the effect of spin-orbit coupling as studied by coupled perturbed Kohn-Sham theory. J Chem Phys 2003;118:3939–3948.
84. Belanzoni P, Baerends EJ, Vanasselt S. Langewen PB. Density functional study of magnetic coupling parameters—reconciling theory and experiment for the TiF3 complex. J Phys Chem 1995;99:13094–13102.
85. Munzarova ML, Kubacek P, Kaupp M. Mechanisms of EPR hyperfine coupling in transition metal complexes. J Am Chem Soc 2000; 122:11900–11913.
86. Abragam A, Bleaney B. Electron paramagnetic resonance of transition ions. Oxford, UK: Clarendon Press; 1970.
87. Carl PJ, Isley SL, Larsen SC. Combining theory and experiment to interpret the EPR spectra of VO21-exchanged zeolites. J Phys Chem A 2001;105:4563–4573.
88. Saladino AC, Larsen SC. Density functional theory calculations of the electron paramagnetic resonance parameters for VO2+ complexes. J Phys Chem A 2003;107:1872–1878.
89. van Lenthe E, Wormer PES, van der Avoird A. Density functional calculations of molecular g-tensors in the zero-order regular approximation for relativistic effects. J Chem Phys 1997;107:2488–2498.
90. Munzarova M, Kaupp M. A critical validation of density functional and coupled-cluster approaches for the calculation of EPR hyperfine coupling constants in transition metal complexes. J Phys Chem A 1999;103:9966–9983.
91. Saladino AC, Larsen SC. Computational study of the effect of the imidazole ring orientation on the EPR parameters for vanadyl-imidazole complexes. J Phys Chem A 2002;106:10444–10451.
92. Saladino AC, Larsen SC. Density functional theory calculations of nitrogen hyperfine and quadrupole coupling constants in Oxovanadium(IV) complexes. J Phys Chem A 2003;107:4735–4740.
93. Stein M, van Lenthe E, Baerends EJ, Lubitz W. g- and a-tensor calculations in the zero-order approximation for relativistic effects of Ni complexes Ni(mnt)(2)(−) and Ni(CO)(3)H as model complexes for the active center of [NiFe]-hydrogenase. J Phys Chem A 2001;105:416–425.
94. Schreckenbach G, Ziegler T. Calculation of the g-tensor of electron paramagnetic resonance spectroscopy using gauge-including atomic orbitals and density functional theory. J Phys Chem A 1997;101:3388–3399.
95. Patchkovskii S, Ziegler T. Calculation of the EPR g-tensors of high-spin radicals with density functional theory. J Phys Chem A 2001;105:5490–5497.
96. Kaupp M, Reviakine R, Malkina OL, Arbuznikov A, Schimmelpfennig B, Malkin VG. Calculation of electronic g-tensors for transition metal complexes using hybrid density functionals and atomic meanfield spin-orbit operators. J Comput Chem 2002;23:794–803.
97. Neese F. Configuration interaction calculation of electronic g tensors in transition metal complexes. Int J Quantum Chem 2001;83: 104–114.
98. Rinkevicius Z, Telyatnyk L, Salek P, Vahtras O, Agren H. Restricted density-functional linear response theory calculations of electronic g-tensors. J Chem Phys 2003;119:10489–10496.
99. Shmerling D, Hegyi I, Fischer M, Blattler T, Brandner S, Gotz J, Rulicke T, Flechsig E, Cozzio A, von Mering C, Hangartner C, Aguzzi A, Weissmann C. Expression of amino-terminally truncated PrP in the mouse leading to ataxia and specific cerebellar lesions. Cell 1998;93:203–214.
100. Bocharova OV, Breydo L, Salnikov VV, Baskakov IV. Copper(II) inhibits in vitro conversion of prion protein into amyloid fibrils. Biochemistry 2005;44:6776–6787.
101. McKinley MP, Masiarz FR, Prusiner SB. Reversible chemical modification of the scrapie agent. Science 1981;214:1259–1261.
102. Cervenakova L, Buetefisch C, Lee HS, Taller I, Stone G, Gibbs CJ, Brown P, Hallett M, Goldfarb LG. Novel PRNP sequence variant associated with familial encephalopathy. Am J Med Genet 1999;88: 653–656.
103. Thompson A, White AR, McLean C, Masters CL, Cappai R, Barrow CJ. Amyloidgenicity and neurotoxicity of peptides corresponding to the helical regions of PrPC. J Neurosci Res 2000;62:293–301.
104. Bosques CJ, Imperiali B. The interplay of glycosylation and disulfide formation influences fibrillization in a prion protein fragment. Proc Natl Acad Sci USA 2003;100:7593–7598.
105. Kuwata K, Li H, Yamada H Legname G, Prusiner SB, Akasaka K, James TL. Locally disordered conformer of the hamster prion protein: a crucial intermediate to PrPSc? Biochemistry 2002;41:12277–12283.
106. Kuwata K, Kamatari YO, Akasaka K, James TL. Slow conformational dynamics in the hamster prion protein. Biochemistry 2004; 43:4439–4446.

 DOI 10.1002/prot